Journal of Sound and Vibration (1999) **228**(3), 511–541
Article No. jsvi.1999.2426, available online at http://www.idealibrary.com onlogo IDEAL®

THE INTERACTION OF PERTURBED VORTEX RINGS AND ITS SOUND GENERATION. PART II

N. W. M. Ko, R. C. K. Leung† and C. C. K. Tang

Department of Mechanical Engineering, The University of Hong Kong, Hong Kong, People's Republic of China

(*Received* 22 *July* 1998, *and in final form* 24 *May* 1999)

The present work extends the study of interactions of two coaxial vortex rings of thin cores with azimuthal instability to wavenumber range $6 \leqslant m \leqslant 11$. Unstable modes are found at $6 \leqslant m \leqslant 10$. Stable mode is found only at $m = 11$. The present range of unstable wavenumbers $m = 1, 2, 5$ to 10 of the two interacting vortices is wider than $m^* = 8$ of a single vortex ring of the same property of core structure. Besides the category of stable mode, two other categories of the unstable mode, namely the odd-m and even-m modes, are classified. The odd-m unstable mode of $m = 5, 7$ and 9 concerns the evolution of star-like structure of one vortex ring with tail sheaths trailing behind. This unstable mode has slower evolution and becomes unstable after the third slip through. The even-m unstable mode of $m = 6, 8$ and 10 more rapid evolution and becomes unstable after the second slip through. Either one ($m = 8$ and 10) or two ($m = 6$) interacting vortex rings evolve into star-like structure with roll- shape sheaths. At $m = 8$, the unstable mode $m^* = 8$ of a single vortex ring, besides the evolution of the roll-shape structure, sheaths wrapping the rolls are also found. Although quadrupole sound radiation is still observed, the far field sound pressure fluctuations depend on the interaction modes, with the roll-shape one (even-m mode) generally the highest, followed by the tail shape one (odd-m mode). The criterion for the onset of unstable mode established in the previous study is also confirmed for the higher wavenumbers.

1. INTRODUCTION

In the previous study [1], based on the vortex blob method [2] and acoustic analogy [3], interactions of two coaxial vortex rings of thin cores with and without azimuthal instability of wavenumbers $1 \leqslant m \leqslant 5$, where m is the number of wave along the vortex, have been investigated numerically. The far field sound generated by these interacting vortex rings of weak axial and radial sinusoidal perturbations was also studied. The behaviour and the far field sound radiated by the two perturbed vortices during the slip throughs of $3 \leqslant m \leqslant 4$ and during the first slip

†Now at the Department of Mechanical Engineering, The Hong Kong Polytechnic University, Hunghom, Kowloon, Hong Kong.

0022-460X/99/480511 + 31 $30.00/0

through of $1 \leqslant m \leqslant 5$ are the same as those of the unperturbed case ($m = 0$). Because of their mutual induction, an unstable mode of the trailing vortex is found during the third slip through at $m = 1$ and 5, significantly lower wavenumbers compared with the unstable mode wavenumber $m^* = 7$ of Widnall and Sullivan [4], $m^* = 8$ of Kino and Ghoniem [2] and $m^* = 8$ of a single vortex ring [1]. The far field sound radiated and their directivity, though still quadrupole, are different from those of the unperturbed cases [1,4].

Based on the normalized streamwise amplitude of the initially trailing vortex, its continuous increase in the peak amplitude suggests a critical streamwise amplitude beyond which the exponential growth and unstable mode are found [1]. The critical amplitude is established at about 5, beyond which there is the formation of hairpin vortices on the trailing vortex, agreeing with that of single vortex [2].

As the first part of the study concerned the wavenumbers $0 \leqslant m \leqslant 5$, the interaction and farfield pressure characteristics at higher wavenumbers have not been investigated. Thus, this part of the study aimed at the understanding of the interacting perturbed vortex rings at high wavenumbers $6 \leqslant m \leqslant 11$ and their far field sound generation.

2. MATHEMATICAL FORMULATION AND NUMERICAL METHOD

As the details of the mathematical formulation and numerical method have been presented [1], only the important ones are shown in the following sections.

The initial perturbation of each thin vortex ring is taken to be

$$\mathbf{Y} = (R + \rho_r e^{im\theta})\mathbf{e}_r + (z + \rho_z e^{im\theta})\mathbf{e}_z, \tag{1}$$

where $\mathbf{e}_r$ and $\mathbf{e}_z$ are unit vectors in the radial and streamwise directions, θ is the azimuthal angle, R is the radius of an unperturbed ring, z is the initial streamwise distance from a reference frame and m is the integer wavenumber of complete waves along the filament periphery (Figure 1). The respective radial and streamwise perturbation amplitudes, ρ_r and ρ_z, are assumed to be very small compared with the ring radius, i.e. $|\rho_r|, |\rho_z| \ll R$.

Based on the concept of identical linear hydrodynamic impulse $\mathbf{I}$ [5] to its perturbed counterpart, the streamwise position z_{CA} and radius r_{CA} are constructed in accordance with the formulae of Batchelor [6] and Saffman [5] as

$$(0, 0, z_{CA}) = \frac{1}{2}\oint \Gamma \frac{\mathbf{y}(s) \times \partial \mathbf{y}(s)/\partial s}{|\mathbf{I}|^2} \cdot \mathbf{I}\mathbf{y}(s)\, \mathrm{d}s \tag{2}$$

and

$$|\mathbf{I}| = \pi r_{CA}^2 \Gamma.$$

In the case of unperturbed vortex rings, z_{CA} and r_{CA} reduce to the streamwise position and radius of the vortices. As the z_{CA} and r_{CA} average out the details of the vortices during their interaction, they only indicate the global trend of the rings.

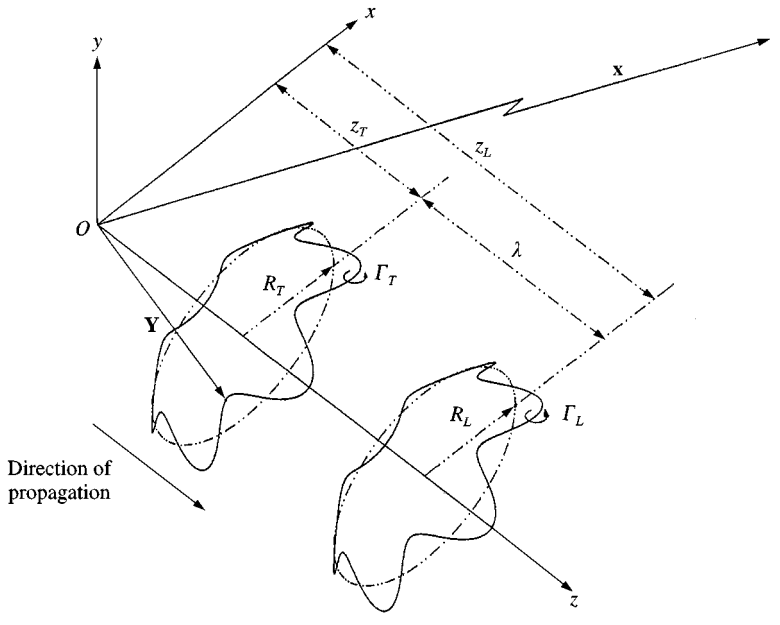

Figure 1. Schematic diagram of the two perturbed vortex rings of thin core.

The velocity V_{CA} and acceleration $æ_{CA}$ are calculated by differentiating equation (2) with respect to time:

$$V_{CA} = (V_z, V_r) = \frac{\mathrm{d}}{\mathrm{d}t}(z_{CA}, r_{CA}) \tag{3}$$

and

$$æ_{CA} = (æ_z, æ_r) = \frac{\mathrm{d}^2}{\mathrm{d}t^2}(z_{CA}, r_{CA}).$$

Based on the three-dimensional vortex blob methods [2,7], the discretized Biot Savart Law is

$$\mathbf{u}_\omega(\mathbf{y}, t) = -\frac{1}{4\pi}\sum_\alpha \Gamma_\alpha \frac{(\mathbf{y} - \mathbf{y}_\alpha)\times \delta\mathbf{s}_\alpha}{|\mathbf{y} - \mathbf{y}_\alpha|^3}\chi\left(\frac{|\mathbf{y} - \mathbf{y}_\alpha|}{\delta}\right), \tag{4}$$

where

$$\chi(r) = 4\pi\int_0^r \xi(\eta)\eta^2\,\mathrm{d}\eta = \frac{r^3(r^2 + 5/2)}{(r^2 + 1)^{5/2}}. \tag{5}$$

The discretized Möhring's sound pressure fluctuation formula [3] is

$$p(\mathbf{x}) = \frac{\rho_0}{12\pi c_0^2|\,\mathbf{x}|^3}\frac{\partial^3}{\partial t^3}\left\{\sum_\alpha \Gamma_\alpha(\mathbf{x}\cdot\mathbf{y}_\alpha)\mathbf{x}\cdot(\mathbf{y}_\alpha\times\delta\mathbf{s}_\alpha) - \frac{1}{3}\sigma^2\varepsilon\mathbf{x}\cdot\boldsymbol{\Omega}\times\mathbf{x}\right\}, \tag{6}$$

where $\varepsilon = 4\pi\int_0^\infty \xi(r)r^4\,\mathrm{d}r = 3/2$ and $\Omega = \sum_\alpha \Gamma_\alpha \delta s_\alpha$, which is zero in unbounded inviscid flow.

The two identical perturbed vortex rings have the following properties: circulation $\Gamma = 1{\cdot}0$, core to the unperturbed ring radius $\sigma/R = 0{\cdot}2$, in phase perturbation $\rho_r/R = \rho_z/R = 0{\cdot}02$ and initial separation $\lambda/R_T = 1{\cdot}0$ (Figure 1). The suffixes L and T denote, respectively, the initially leading and trailing vortex rings. The range of wavenumbers is $6 \leqslant m \leqslant 11$. The far field pressures are evaluated at a radial distance $120R_T$. The normalized length $x' = x/R_T$, $t' = \Gamma_T t/R_T^2$; pressure $p' = p/(\Gamma_T/R_T)^2$ for unity density and circulation $\Gamma' = \Gamma/\Gamma_T$. The allowable error of the total vorticity and the linear vorticity impulse of the potential vortex motions is kept within 2%.

3. RESULTS AND DISCUSSIONS

3.1. EVOLUTION OF PERTURBED VORTEX INTERACTION MODE

Perturbed at $m = 6$, the two vortex rings during the first slip through do not indicate significant difference from those of the unperturbed ones ($m = 0$). Thus, they are not presented. During the second slip through at $t' = 11{\cdot}3$, the trailing vortex (the initial leading vortex) slips through the leading vortex (the initially trailing vortex), which evolves into a star-like vortical structure with the formation of thin sheaths of vortical material (not shown here). The trailing vortex (the initially leading vortex) also has an amplitude as large as that of the leading vortex and begins to form a star-like vortical structure. At $t' = 13{\cdot}575$, both vortex rings have six this sheaths appearing as "rolls" of vortical materials (Figure 2(a)). The six thin sheath rolls of the initially leading vortex appear at the azimuthal positions of the initial perturbation wave peaks, whereas those of the initially trailing vortex appear at the valleys. They are antiphase with those of the initially leading vortex. The peaks of the waves of the former form protruding portions, extending towards the interior of the leading vortex due to their strong mutual induction and the tendency of undergoing further slip through.

The formation of the sheaths starts with the radial growth at $t' \approx 8$ of the initially trailing vortex before the second slip through and the high streamwise and radial growth rates, $\mathrm{d}\Delta z'/\mathrm{d}t'$ and $\mathrm{d}\Delta r'/\mathrm{d}t'$ respectively, of the initially trailing vortex and then the initially leading vortex near the slip through (Figures 3(a) and 3(b)). The sheaths of the initially leading vortex appear after the second slip through, at which both its streamwise and radial growth rates increase rapidly (Figures 3(a) and 3(b)).

The evolution of the two perturbed vortex rings is significantly different from that of $m = 5$. For $m = 6$, both vortex rings develop thin sheaths of vortical structures rolling around the vortices soon after the second slip through and their roll-shape thin sheaths are different from the long tails trailing only behind the trailing vortex ring of $m = 5$, while the leading ring does not develop into a star-like structure [1].

For $m = 7$, the perturbed rings during the third slip through at $t' = 18{\cdot}575$ are shown in Figure 2(b). The trailing vortex (the initially trailing vortex) becomes a star-like structure with seven long tails of hairpin vortices trailing behind the ring, while the comparatively more stable leading vortex (the initially leading vortex) shows no appreciable growth of perturbation. The sheaths of vortical material at

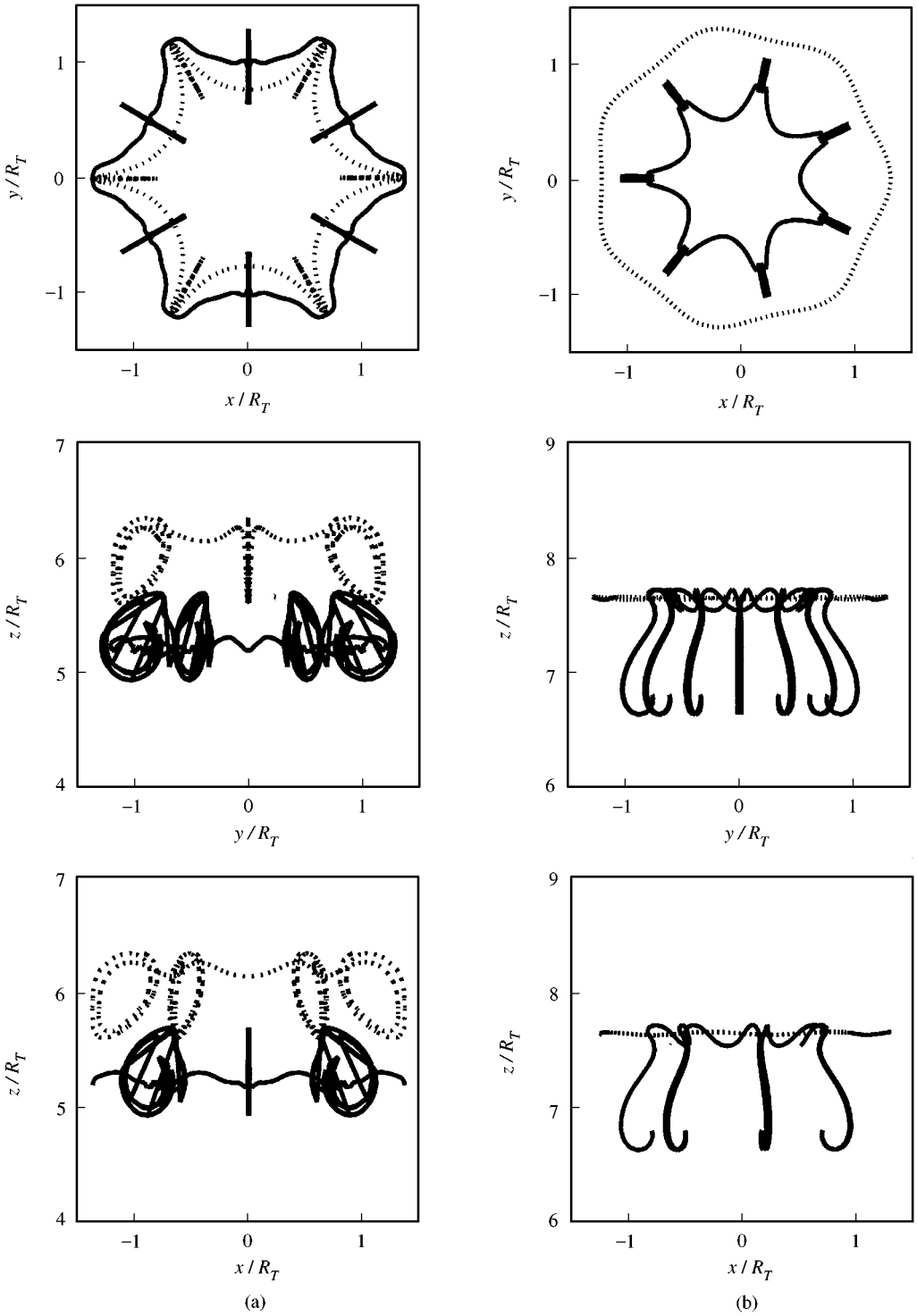

Figure 2. Interaction of the two perturbed vortex rings. (a) $m = 6$, $t' = 13{\cdot}575$; (b) $m = 7$, $t' = 18{\cdot}575$; (c) $m = 8$, $t' = 13{\cdot}5$; (d) $m = 9$, $t' = 18{\cdot}275$; (e) $m = 10$, $t' = 15{\cdot}4$; (f) $m = 11$, $t' = 18{\cdot}575$. ——, Initially trailing vortex; ·····, initially leading vortex.

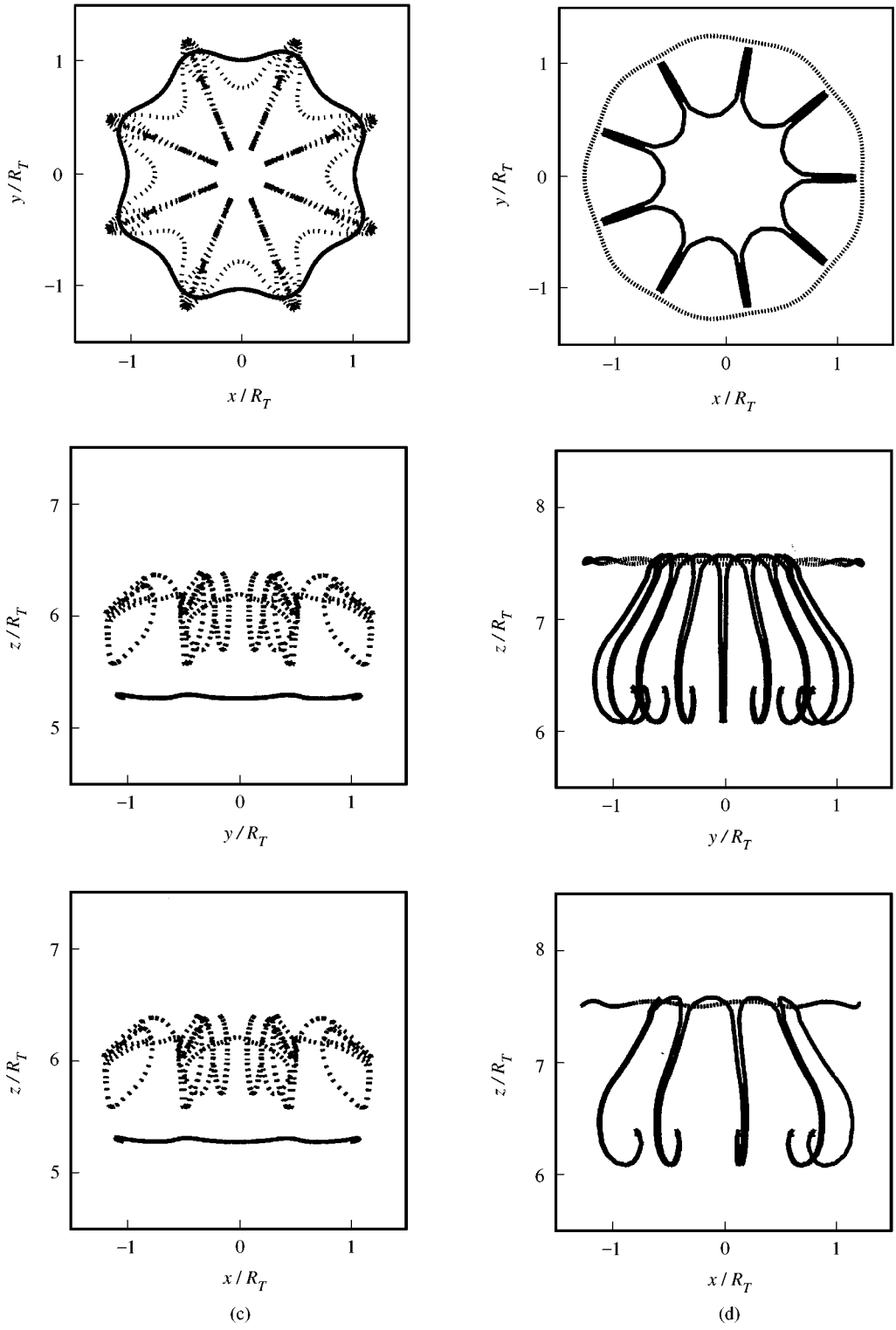

Figure 2. Continued.

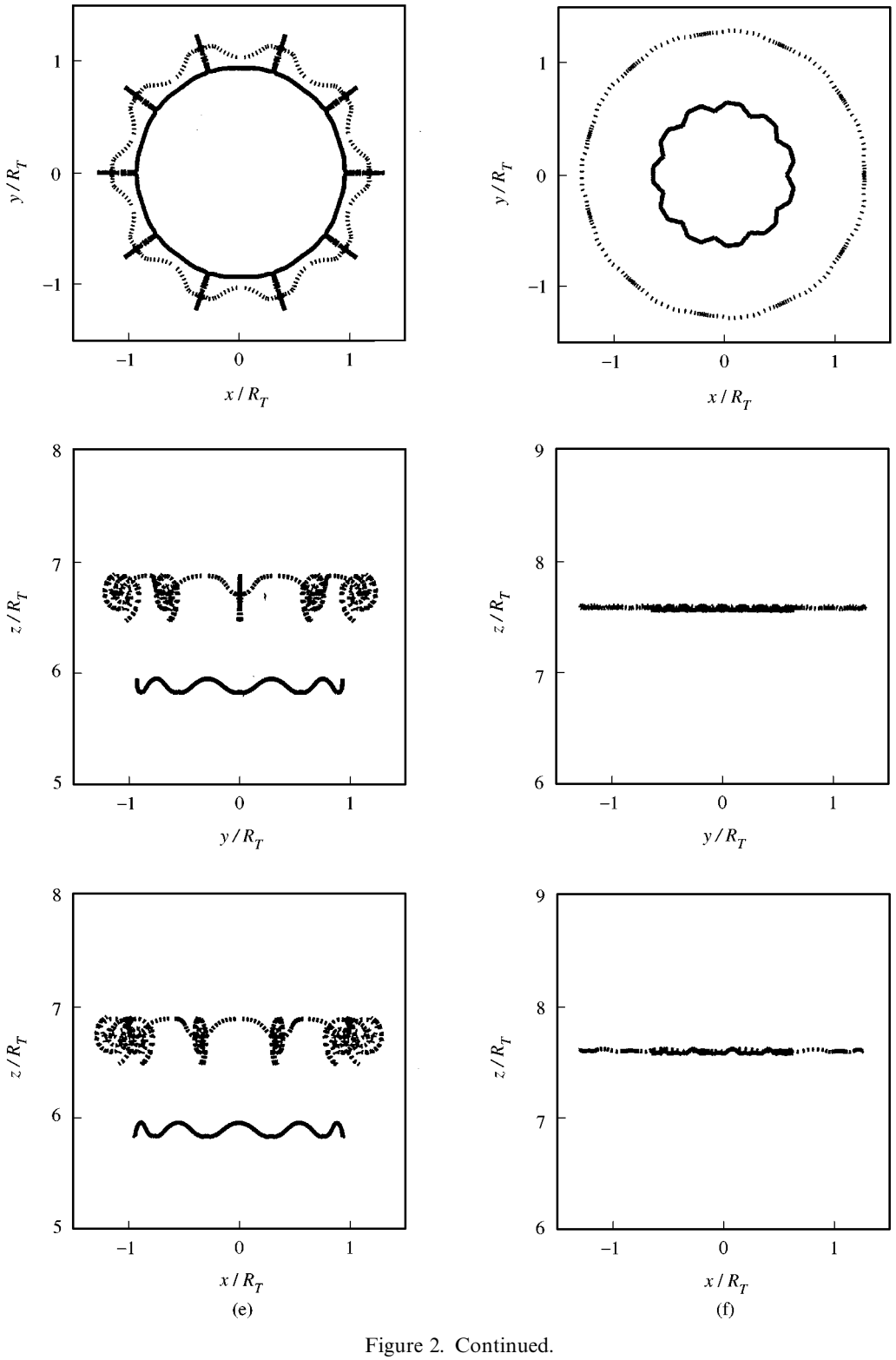

Figure 2. Continued.

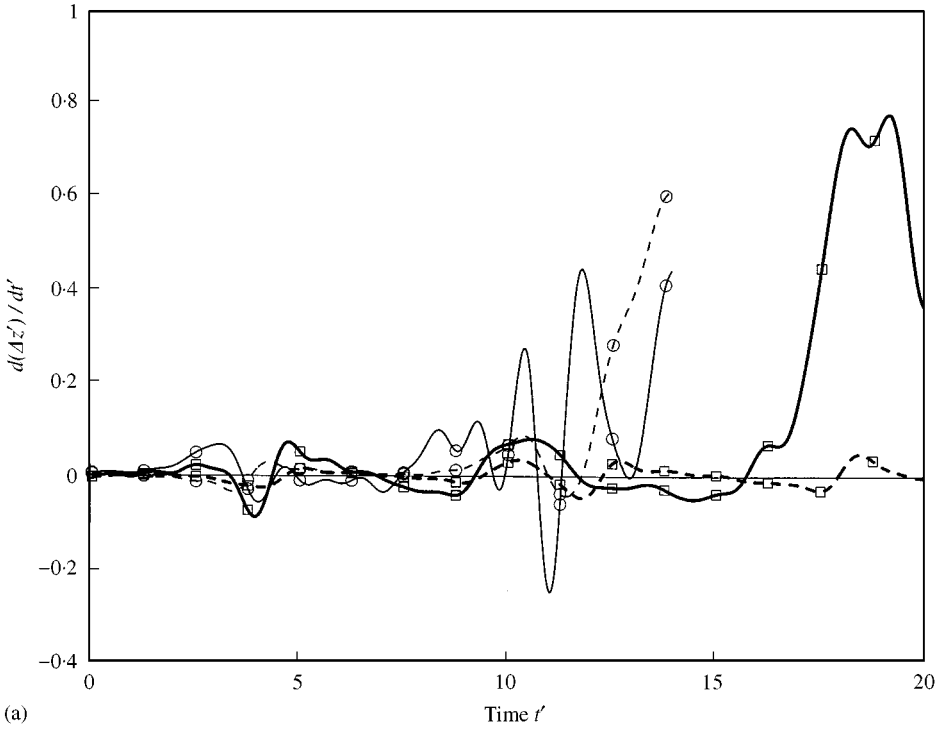

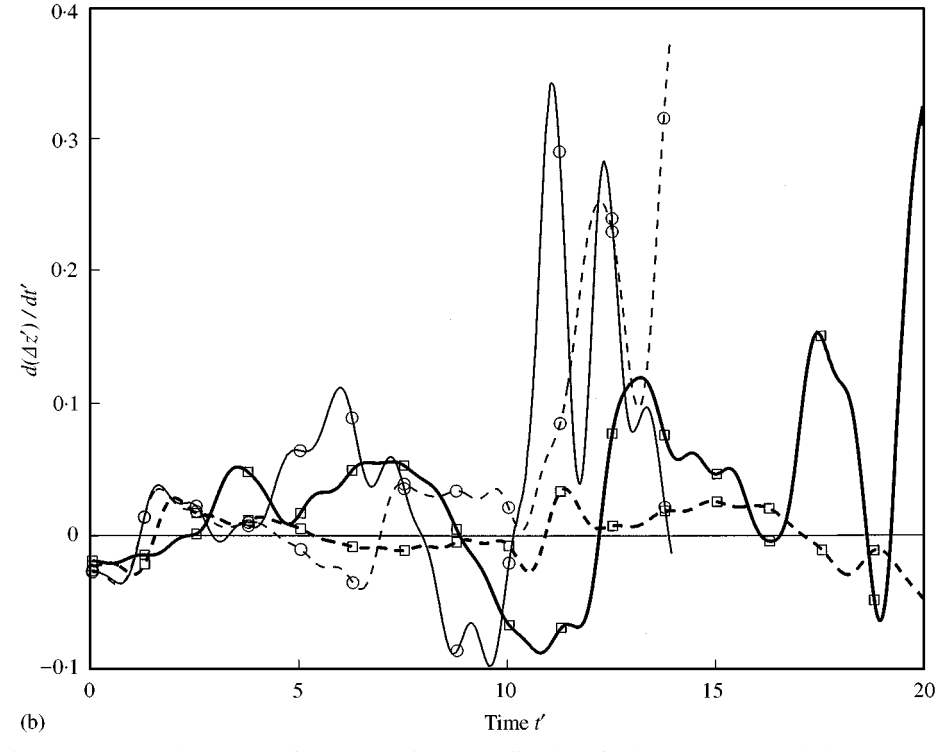

Figure 3. Growth rates of perturbation amplitude of the two perturbed vortex rings. (a) Streamwise; (b) radial. ○, $m = 6$; □, $m = 7$. ——, Initially trailing vortex; – – – initially leading vortex.

the third slip through are also indicated by the large streamwise growth rate (Figure 3(a)), while the radial growth rate is lower in magnitude (Figure 3(b)). The perturbation waves of the two vortex rings are out of phase. Apart from the absence of the high-frequency perturbation on the unstable vortex, the star-like structure of this wavenumber $m = 7$ is nearly the same as that of the unstable wavenumber $m = 5$[1], but different from those of $m = 6$ (Figure 2(a)).

For $m = 8$, due to the rapid increase in the numerical error, computation was terminated at $t' = 13{\cdot}8$. At $t' = 13{\cdot}5$, soon after the second slip through, the initially leading vortex has developed into a roll-shaped vortical structure, while the initially trailing vortex still maintains its original shape (Figure 2(c)). Although it is basically of roll-shape, the sheaths seem to be divided into two parts. One appears as the beginning of the formation of the thin sheath while the other as the roll. The streamwise and radial growth rates indicate the rapid evolution of the initially leading vortex during the second slip through (Figures 4(a) and 4(b)), with the former greater than the latter.

For $m = 9$, perturbed rings during the third slip through at $t' = 18{\cdot}275$ are shown in Figure 2(d). The trailing vortex (the initially trailing vortex) becomes a star-like structure with nine long tails trailing behind the ring, while the leading vortex (the initial leading vortex) is still stable. The star-like ring structure of this wavenumber $m = 9$ is similar to those of $m = 7$ (Figure 2(b)) and 5 [1] with the length of the tail of about $1R_T$–$1{\cdot}5R_T$. The streamwise and radial growth rates of the initially leading and trailing vortices are shown in Figures 4(a) and 4(b) respectively. The rapid increase in both the growth rates of the trailing vortex (the initially trailing vortex) at $t' > 16$ is associated with the formation of the tails at the third slip through.

For $m = 10$, computation was terminated at $t' \approx 15{\cdot}5$, after the second slip through at $t' = 11$. At $t' = 15{\cdot}4$, the initially leading vortex, after slipping through the initially trailing vortex, develops the roll-shape sheaths (Figure 2(e)). These sheaths appear at the peaks of the waves. The initially trailing vortex indicates some unstable behaviour, but still maintains its original circular shape with perturbation. The roll-shape sheaths of the initially leading vortex are similar to those of $m = 6$ and 8 (Figures 2(a) and 2(c)), but different from those of the long tail of $m = 5$, 7 and 9 (Figures 2(b) and 2(d)). The roll-shape structure is associated with the rapid increase in both the streamwise and radial growth rates of the initially leading vortex at $t' > 11$ (Figures 5(a) and 5(b)).

For $m = 11$, even at the third slip through instant, the two perturbed rings are still stable, although the trailing vortex (initially trailing vortex) indicates perturbation (Figure 2(f)). The streamwise and radial growth rates at $0 \leqslant t' \leqslant 20$ are low, not significantly different among the three slip throughs (Figures 5(a) and 5(b)).

Together with the previous findings [1], the present study reveals the very complicated interaction of the two weakly perturbed thin vortex rings of wavenumbers $1 \leqslant m \leqslant 11$. Based on the characteristics of the vortex interaction, the present study establishes three modes of interaction of the two weakly perturbed vortex rings. The first one is the stable mode with wavenumbers $m = 3$, 4 and 11. In the stable mode, the interacting vortices show no severe distortion due

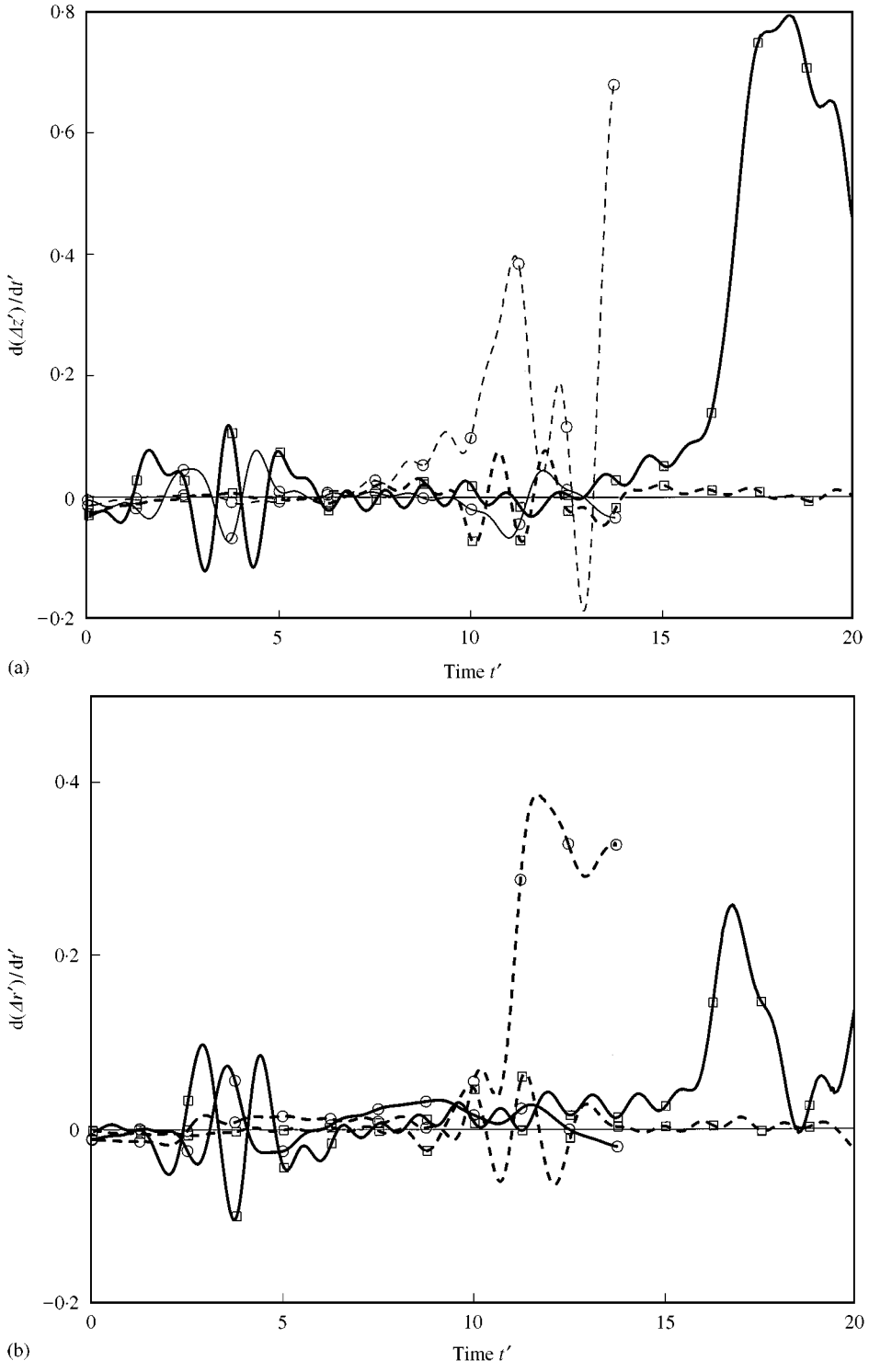

Figure 4. Growth rates of perturbation amplitude of the two perturbed vortex rings. (a) Streamwise; (b) radial. ○, $m = 8$; □, $m = 9$. ——, Initially trailing vortex; – – –, initially leading vortex.

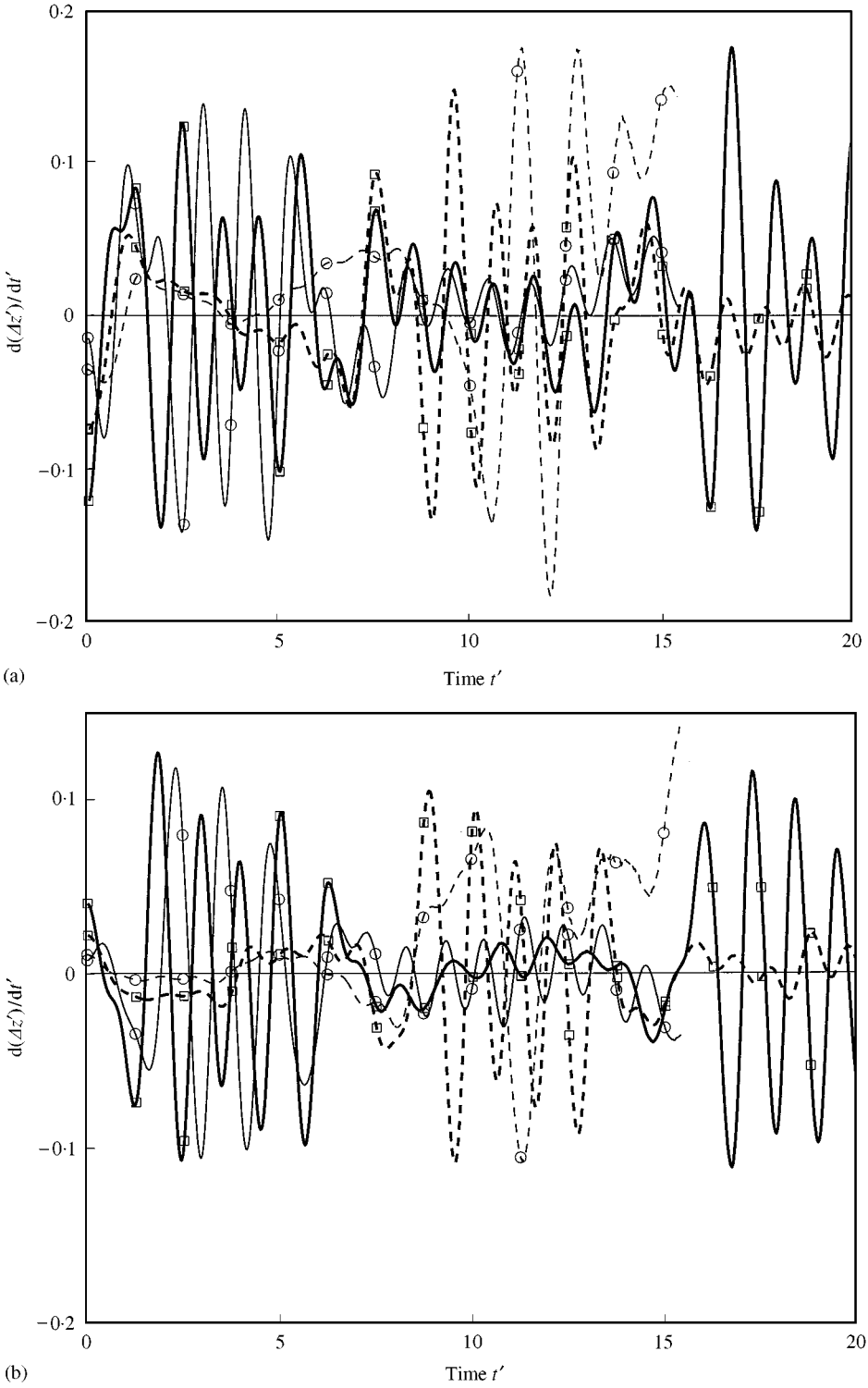

Figure 5. Growth rates of perturbation amplitude of the two perturbed vortex rings. (a) Streamwise; (b) radial. ○, $m = 10$; □, $m = 11$. ——, Initially trailing vortex; – – –, initially leading vortex.

to perturbation and their amplitudes and growth rates of the perturbation waves during the three slip throughs are basically the same.

The second mode concerns the unstable interaction of vortex rings perturbed at the wavenumbers $m = 5$, 7 and 9. This is denoted as the odd-m unstable mode. The trailing vortex (the initially trailing vortex) becomes unstable at the third slip through, while the leading (the initially leading vortex) is still stable. The unstable trailing vortex ring develops into a star-like vortical structure with long tails of hairpin vortices trailing behind (Figures 2(b) and 2(d)). The number of tails and their length vary with wavenumber. The evolution of the unstable trailing vortex is associated with the rapid increase in its streamwise and radial growth rates.

The third mode, denoted as the even-m unstable mode, concerns the unstable interaction of vortex rings perturbed at the wavenumbers $m = 6$ and 10. In this unstable mode, computation was terminated shortly after the second slip through at $t' \approx 15$, due to the rapid increase in the numerical error since the present numerical model cannot accurately resolve the interaction of very peaky and closely spaced vortical strips, formed by the two closely counter rotating vortical segments connected at one end. The stretching and rolling around the vortex ring lead to the appearance of roll-shape sheaths. For $m = 6$, at $t' = 13{\cdot}575$, both the initially leading and trailing vortex rings evolve into the roll-shape structure (Figure 2(a)). The roll-shape sheaths of the two vortex rings are antiphase. The sheaths of the initially leading vortex are on the peaks of the waves, whereas those of the initially trailing vortex are on the valleys of the waves, with their peaks forming protrusions. For $m = 10$, at $t' = 15{\cdot}4$, only the initially leading vortex has roll-shape sheaths on the peaks of the waves, while the initially trailing vortex has not yet developed any sheath (Figure 2(e)).

For the unstable mode of $m = 8$, computation was also terminated shortly after the second slip through $t' \approx 14$. The slip through trailing vortex (the initially leading vortex) evolves into the roll-shape structure and forms thin sheaths (Figure 2(c)). However, the leading vortex (the initially trailing vortex) remains stable, without any appreciable sheath growth or severe vortex stretching. This suggests that the more preferred mode of evolution is that of the roll-shape type and this $m = 8$ is also classified into the even-m unstable mode.

For a single laminar vortex ring, based on the present parameters, the estimated wavenumber for the unstable mode is $m^* = 8$ [1], in comparison with $m^* = 7$ [4] and $m^* = 8$ [2]. However, the unstable wavenumber also shows dependence on the Reynolds number in experiments [8–11]. It varies from $m^* = 4$ or 5 at $\mathrm{Re} \approx 1150$ to 6 or 7 at 1650. For the turbulent vortex ring, the unstable wavenumber increases to $m^* = 8$ at $\mathrm{Re} = 7500$ [12]. Thus, the individual vortices, by themselves, of $1 \leqslant m \leqslant 7$ and $9 \leqslant m \leqslant 11$ of the present study are within the linear stable regime [4]. In this regime the peak to peak amplitudes and their growth rates in both the streamwise and radial directions are not amplified [1].

In the present study the two interacting perturbed rings are also within the linear stable regime at the wavenumbers of $m = 3$, 4 and 11 at $t' \leqslant 20$, undergoing three slip throughs. For $m = 11$, the normalized streamwise and radial perturbation amplitudes (peak to peak) of both interacting trailing and leading vortices remain

bounded, with values less than 2·4 (Figures 6(a) and 6(b)). This observation is consistent with the criterion of critical streamwise normalized amplitude of 5 [1], beyond which the vortex exhibits an exponential instability growth. The importance of the streamwise perturbation, rather than the radial one, during instability development is also implied by the fact that the streamwise vorticity tends to amplify the initial azimuthal perturbation, thereby leading to a rapid growth of the three dimensionality [13].

Unstable mode is also found at the other wavenumbers. Except the lowest wavenumber $m = 1$ (not yet categorized), in the interaction of vortices perturbed at the odd-m unstable wavenumbers, the linear stage, the non-linear stage and the violent stretching of the counter rotating hairpin vortices [2] are also found on the trailing vortex (the initially trailing vortex) (Figures 2(b) and 2(d)). The leading vortex (the initially leading vortex) is still stable, even after the third slip through. For the trailing vortices, during the third slip through, the folding backwards and the highly stretched hairpin vortices of the trailing vortex towards the original axis appear as tails and are much more highly stretched than those of the single vortex [2]. The tail sheath is also shown by the flow visualization results of a single vortex ring at the wavenumber $m = 7$ [4]. The length of the present tail sheath is long, about $1R_T$ at $x' = 7{\cdot}6$ of the perturbed interacting vortex rings at $m = 7$ (Figure 2b). The tails of $m = 5$ and 9 are even more stretched, with their length approximately equal to $1{\cdot}5R_T$, indicating the difference in the induction of the vortex filaments of different wavenumbers in the odd-m unstable mode.

The streamwise and radial amplitudes of the two vortices at the wavenumbers of odd-m unstable mode are shown in Figures 7(a) and 7(b) respectively. The initially leading vortex, even after three slip throughs, is still stable with low normalized streamwise amplitude less than 4. The initially trailing vortex, however, exhibits a progressive increase in the amplitude after each slip through. Just before the third slip through, the critical normalized streamwise amplitude of about 5 is exceeded by the initially trailing vortex of these three odd wavenumbers. Beyond the critical time, which varies from $t^* \approx 16$ to 17, the streamwise amplitude grows exponentially, resulting in the tails of the highly stretched vortices.

As discussed earlier, for single vortex ring the critical streamwise amplitude seems to be about 1·8 [1, 2]. For the two interacting vortices of the odd-m unstable mode, the critical streamwise amplitude increases to about 5. This suggests that with the presence of another vortex and their mutual interaction, the higher critical amplitude implies that the interaction and slip through tend to stabilize the evolution, and it is at higher amplitude before exponential growth begins. This may be due to the stabilization effect of the acceleration of the trailing vortex during its slip through of the leading vortex.

The interacting vortices perturbed at the even-m unstable wavenumbers also indicate violent vortex stretching of the vortex filament (Figures 2(a), 2(c) and 2(e)). Such violent stretching occurs not only on the trailing vortex of wavenumbers $m = 8$ and 10, but also on both the leading and trailing vortex rings of $m = 6$. Instead of the appearance of the tails in the odd-m unstable mode, the thin sheaths of this unstable mode are of roll-shape, trailing behind the vortex. The occurrence of these roll-shapes sheaths during the second slip

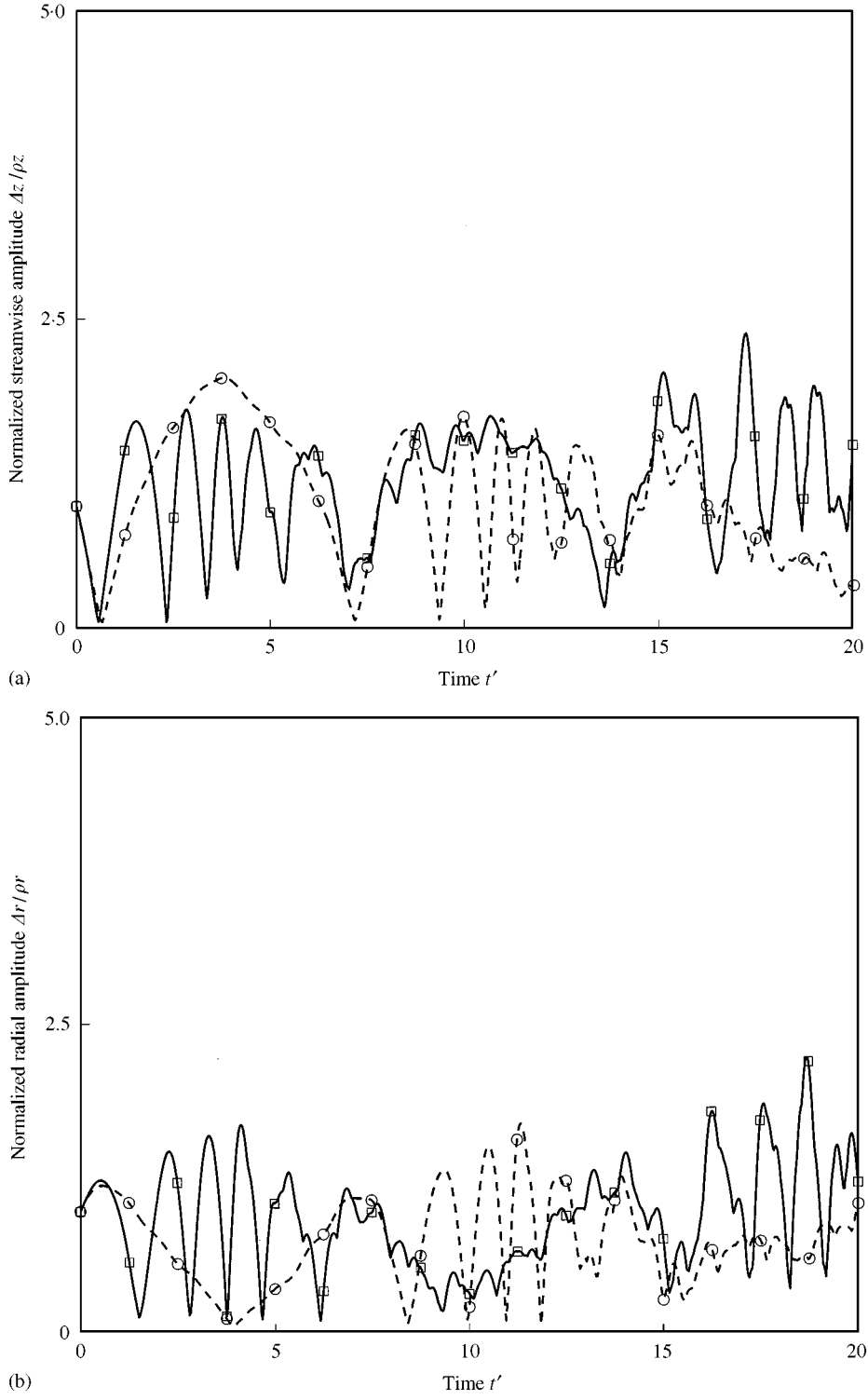

Figure 6. Normalized peak to peak perturbation amplitudes of the interacting vortex rings of stable mode $m = 11$. (a) Streamwise; (b) radial. ——, Initially trailing vortex; – – –, initially leading vortex.

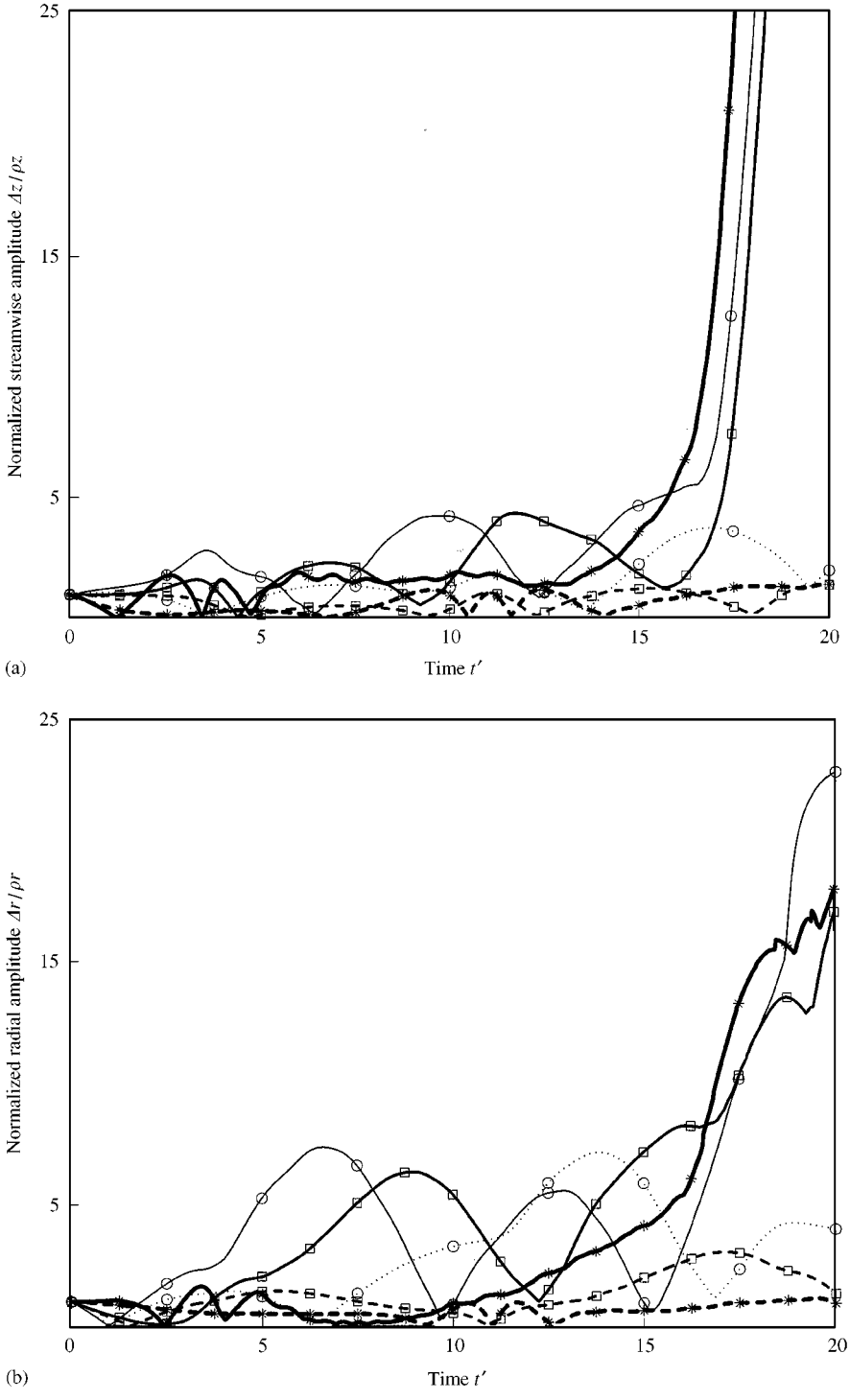

Figure 7. Normalized peak to peak perturbation amplitudes of the interacting vortex rings of odd-m unstable mode. (a) Streamwise; (b) radial. ○, $m = 5$; □, $m = 7$; *, $m = 9$. ——, Initially trailing vortex; – – –, initially leading vortex.

through, earlier than occurrence of tails during the third slip through of the odd-m mode, suggests the earlier evolution of one or both vortices in this unstable mode.

The streamwise and radial amplitudes of the two vortices, as shown in Figures 8(a) and 8(b), respectively, support the above observation. For $m = 8$ and 10, the trailing vortex (the initially leading vortex) has its amplitudes increased soon after the first slip through. For $m = 8$, the streamwise amplitude of the initially leading vortex is greater than the critical amplitude of about 5 at $t' \approx 10$, while for $m = 10$ at $t' \approx 13{\cdot}5$. For $m = 6$, at which wavenumber both vortex rings form into roll-shape, the critical amplitude reached is $t' \approx 9$ for the initially trailing vortex. This indicates that the initially trailing vortex experiences more violent evolution than the initially leading one and is associated with its higher growth rates (Figures 3(a) and 3(b)).

The above observations of the vortex evolution of the odd-m and even-m unstable modes also support the validity of the criterion of the normalized streamwise perturbation of about 5, beyond which severe vortex stretching occurs. The more unstable mode wavenumbers, leaving the stable wavenumbers to $m = 3$, 4 and 11, suggest the strong effect of the interaction and the mutual induction of perturbated vortex rings of thin core. The induced velocity and the strain field induced by the ring on the perturbation waves affect the stability of the wave of the vortex ring [2]. The additional induction, due to the presence of another vortex ring, also affects more significantly the stability of the interacting vortices. Form the present results, the latter effect of the presence of an additional vortex is so strong that only the wavenumbers $m = 3$, 4 and 11 are still within the stable mode, while the others are unstable. This is significantly different from the instability of a single vortex ring with identical vortex core structure that only one wavenumber $m^* = 8$ is unstable. The isolated single thin core vortex ring is stable to long wavelength perturbations and its instability is normally associated with short wavelength mechanism [8–10].

A vortex ring becomes unstable either by the presence of other vortices or by the other portions of the curved vortex itself. For two coaxial vortex rings at low Reynolds numbers at which successive leapfrogging occurs, there is a tendency for the vortex cores to undergo early development of azimuthal bending instabilities during the first slip through [14]. There are tail sheaths trailing behind the slipped through vortex. The length of the sheath is about one diameter of the ring. These instabilities are developed even though no perturbation was introduced. This means that the leapforgging or slip through process induces instabilities on the two "natural" vortex rings. Unfortunately, the unstable wavenumber of the interacting rings is not available [14].

In the study of a vortex ring impacting a solid boundary, the secondary vortex ring generated develops instability, which grows rapidly due to the vortex stretching and tilting in the presence of the mean strain field generated by the primary vortex ring [15]. Under the combined Biot–Savart effects and their mutual interaction, the stability characteristics are altered and long wave disturbances can grow. Unstable evolution of the secondary vortex ring with $m = 6$ perturbation is observed. Very rapid continuous growth of the axial component occurs at $t' > 3{\cdot}2$,

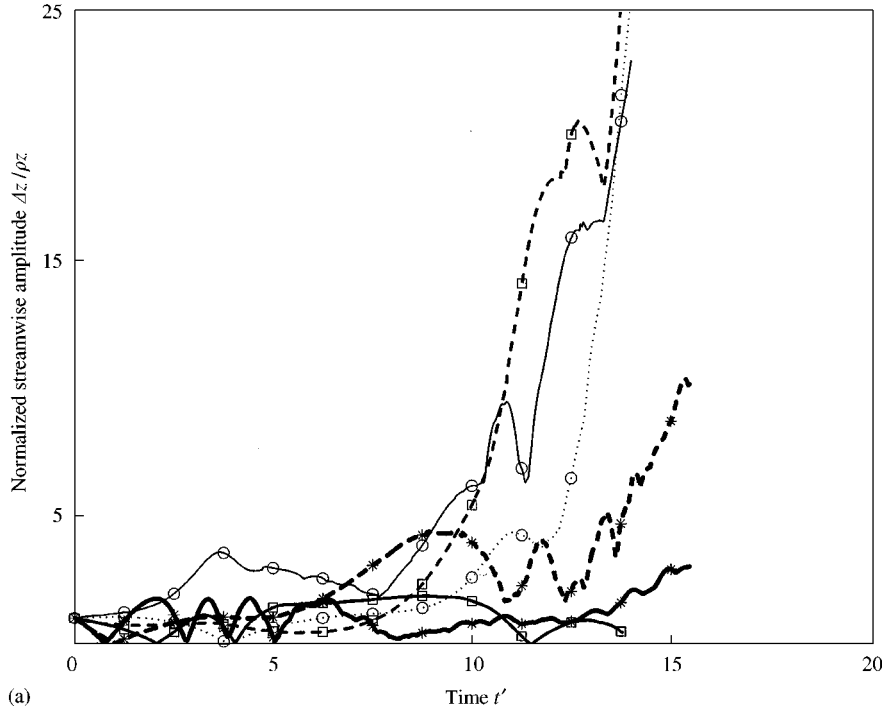

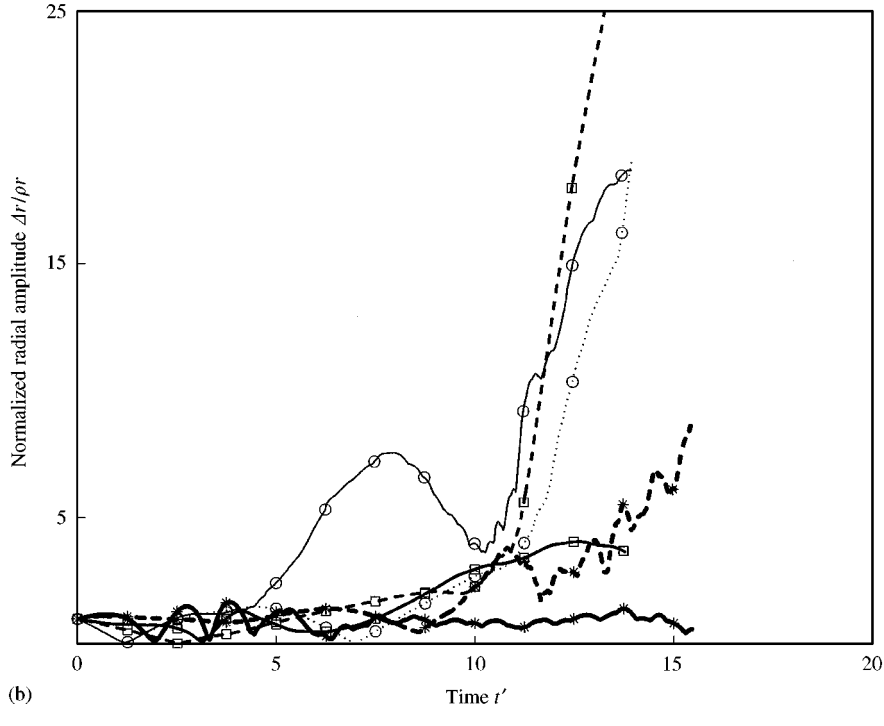

Figure 8. Normalized peak to peak perturbation amplitudes of the interacting vortex rings of even-m unstable mode. (a) Streamwise; (b) radial. ○, $m = 6$; □, $m = 8$; *, $m = 10$. ——, Initially trailing vortex; – – –, initially leading vortex.

while the radial component experiences a drop after the initial growth. At $3{\cdot}2 \leqslant t' \leqslant 4{\cdot}3$, the growth of the axial amplitude of the second vortex amounts to 32 times. This unstable growth at $m = 6$ is in contrast with the isolated thin core vortex ring, which is stable to long wavelength perturbations.

At $x/D = 3$ of an unforced circular jet at $\mathrm{Re} = 10^4$, flow visualization results indicate jets of fluid are shed from regions between vortices [16]. The orderly spaced vortex lobes show a perturbation of wavenumber $m = 8$. For the single vortex ring of similar dimensions and convection velocity, the unstable wavenumber is 9, slightly higher than that of the interacting coherent structures of the jet [16]. At $x/D = 3$, one would expect three slip throughs or coalescence of the initial vortices generated near the nozzle exit. Thus, the interaction of the successive coherent structures results in a lower unstable wavenumber than that of the single vortex ring.

In the flow visualization of periodically excited ring vortices in the transition regime or circular jet (axisymmetric shear layer), streamwise instabilities of both the leading and trailing vortices are found [17]. At $x/D \approx 2$, after the first slip through, the coalesced vortices are more diffused with rapid elongation. The wavenumber of the vortices, though not definitely established, appears to be 6. The flow visualization photograph [17] is similar to that of the two interacting thin core vortices of $m = 6$ of the present numerical study (Figure 2(a)). $m = 6$ is the only wavenumber at which both the leading and trailing vortices are unstable (Table 1). The rapid growth in the streamwise direction after the second slip through instant of both vortices with an amplitude ratio of 2·6 (Figure 8(a)) is comparable with the smoke rings of a ratio of about 1·5 [17].

In a numerical study of a transitional axisymmetric jet subjected to periodic perturbations in both the streamwise and circumferential direction, based on vortex filaments, streamwise subharmonic perturbation results in the pairing of successive vortices [18]. With the additional introduction of a circumferential perturbation of wavenumber of 5, the relative dominance of the global and local induction gives rise to the opposite sign of streamwise vorticity in the braid and ring region. The flow visualization of a weakly forced jet indicates a wavenumber $m = 6$, at which the instability occurs with the presence of the counter-rotating pairs of streamwise vortex tubes [18]. The difference in the wavenumber of five of the numerical simulation and of six of the experimental study may indicate that the more preferred unstable wavenumber of the jet is the latter $m = 6$.

The strongly forced transitional axisymmetric cold jet, forced at a Strouhal number of 0·78, has a wavenumber $m = 8$ and the corresponding number of side jets at $x/D = 4$ [19]. The higher Strouhal number for the excitation was adopted for more stable side jets. The vortex rings experience very rapid evolution from $x/D = 3$ to 4. At the latter position the side jets are well established.

The two laminar vortices of the water jet under axisymmetric forcing at two frequencies have waves on the rings at $x/D \approx 2$, before and after the slip through [20]. The streakline patterns indicate the trailing vortex has bigger streamwise growth than the leading vortex. The leading vortex has a noticeable wavy pattern. The trailing vortex experiences two time increases in its streamwise amplitude soon

TABLE 1

Characteristics of interaction of the unperturbed and perturbed vortex rings of different wavenumbers

		Shape				
m	Mode	Initially leading vortex	Initially trailing vortex	Maximum sound pressure	t'	Occurence of maximum sound pressure
0	Stable	Stable	Stable	$+0{\cdot}03, -0{\cdot}02$	≈ 19	Third slip through
1	Unstable	Ellipsoidal, tilted	Long tail	$+0{\cdot}03, -0{\cdot}02$	≈ 19	Third slip through
2	Unstable	Stable	Unstable	$+0{\cdot}05, -0{\cdot}05$	≈ 19	Third slip through
3	Stable	Stable	Stable	$+0{\cdot}03, -0{\cdot}02$	≈ 19	Third slip through
4	Stable	Stable	Stable	$+0{\cdot}03, -0{\cdot}02$	≈ 19	Third slip through
5	Odd-m unstable	Stable	Star-like, long tail	$+0{\cdot}07, -0{\cdot}06$	≈ 19	Third slip through
6	Even-m unstable	Roll-shape	Roll-shape	$+0{\cdot}27, -0{\cdot}24$	≈ 11	Second slip through
7	Odd-m unstable	Stable	Star-like, long tail	$+0{\cdot}11, -0{\cdot}08$	≈ 19	Third slip through
8	Even-m ustable	Star-like, thin sheath and roll-shape	Stable	$+0{\cdot}08, -0{\cdot}07$	≈ 11	Second slip through
9	Odd-m unstable	Stable	Star-like, long tail	$+0{\cdot}27, -0{\cdot}4$	≈ 17	Third slip through
10	Even-m unstable	Roll-shape	Unstable	$+0{\cdot}18, -0{\cdot}16$	≈ 14	Second slip through
11	Stable	Stable	Stable	$+0{\cdot}03, -0{\cdot}03$	≈ 19	Third slip through

after the slip through and the appearance of the long tails or sheaths or vortical material trailing behind the trailing ring.

By comparing the patterns of the two vortex rings of the second category of odd-m unstable mode, the leading vortex of $m = 7$ and 9 before the third slip through does not have a significant wavy pattern (though the results are not shown here, those during the slip through instant are shown in Figures 2(b) and 2(d)). For $m = 5$, a noticeable wavy pattern of the leading vortex is observed before the third slip through instant [1]. The ratio of the streamwise amplitudes of the trailing to leading vortex at $t' = 17{\cdot}5$ of this wavenumber is about 3. The ratios of $m = 7$ and 9 are about 13 and 16 respectively. The former of $m = 5$ is comparable with that of 1·5 of laminar vortices of excited jet [20]. Further, the trailing vortex streamwise growth before and after the third slip through of the present $m = 5$ amounts to 3·7 times, again comparable with 2 times of the excited jet. The above, thus, suggests that the jet of Paschereit *et al.* [20] is excited at the unstable wavenumber $m = 5$ of the odd-m unstable mode.

With axisymmetric forcing, for the occasional case of no distinct lower mode, both the leading and trailing vortex rings of the water jet have a larger wavy patterns [20]. For the present study, it is only at $m = 6$ that both the vortex rings have shown large wavy patterns before the second slip through (results not shown here) and they are similar to those of the forced water jet [20]. The absence of the long tails and the very diffused and thick vortex rings after the slip through may also suggest the unstable wavenumber of 6 of the excited jet. This further suggests the even-m unstable mode of vortex interaction of the third category, of which roll-shape structures are formed during interaction.

For the air jet of Reynolds number Re_D, based on the nozzle diameter D, of 78 000, axisymmetric forcings at the fundamental frequency and at the fundamental and subharmonic frequencies excite the jet at the unstable mode of $m = 8$ [20]. It is independent of whether it is forced by one or two frequencies. This means that the jet is forced at the $m = 8$ mode. In the present study, the mode of $m = 8$ is also of the third category, of which roll-shape structures are formed (Figure 2(d)). However, at this wavenumber only the trailing vortex undergoes the rapid growth, while the leading one is still stable (Table 1).

In the submerged jet, the number of streamwise structures is a function of Reynolds number [21]. The number of streamwise structures is related and is the same as the number of mode or the most preferred wavenumber of the ring. It is suggested that these structures evolve in the braid region between primary vortical structures. At $x/D = 3{\cdot}5$, they appear as fingers of dyed fluid that emerge from the braid region and stretch around the following vortex. At this position, the vortex core or ring is still distinct, before its loss of identity slightly further downstream.

In the present investigation of thin vortex interaction, for the wavenumber $m = 8$, after the second slip through, the initially leading vortex has the shape of the rolls of vorticity and the sheaths or fingers of vorticity stretching around the rolls (Figure 2(c)). This is not too dissimilar to the flow visualization picture of the preferred mode at the Reynolds number of 5500 [21]. The above agreement may suggest that during the slip through process the vorticity of the vortex itself may also contribute to the formation of the sheaths wrapping around the primary vortices. However, further study will be required for the implication of the present findings in this aspect.

In the smoke visualization study of a forced transitional jet at wavenumber $m = 1$, the two interacting vortex rings, out of the five visualized rings, of the case of roll-up and out-of-plane tilting [22] agree with those of the present findings [1]. The tilting of the leading ring, the distortion and slip through of the leading edge of the trailing ring and their shapes are the same, even though there are another vortex downstream and upstream of the interacting pair.

The results of the above work for the motion of the adjacent vortex rings or successive vortex rings of axisymmetric jet indicate that the unstable mode wavenumbers occur not only on $m^* = 8$ of the single vortex but also on $m = 1$, 5–8, depending on Reynolds number. The flow visualization studies also support the present classification of the interaction mode, based on the development of the tail sheaths and roll-shape structures. The former occurs basically with

interaction of odd number wavenumbers, while the latter of the even ones. The latter also has earlier evolution and exhibits non-linear growth soon after the second slip through, while that of the former after the third slip through. This also indicates the even-m mode is the most preferred mode of perturbed vortex ring interaction.

Both the results of Leung and Ko [1] and the present study show that the dynamics of the vortex ring pairing with the initial weak perturbation are strongly dependent on the wavenumber. The present findings can also be used to explain some of the observations of the coherent structures in circular jet. It is reported that the Strouhal number, based on the jet nozzle diameter and the characteristic passage frequency near the end of the potential core, for the jet column mode or preferred mode, varies from 0·25 to 0·85 [23]. Gutmark and Ho [24] attributed the cause of this discrepancy to the small spatially coherent background disturbances inherent in the experimental facilities. These disturbances are likely to provide the initial perturbations at a particular or group of wavenumbers on the shear layer vortex rings formed immediately downstream of the nozzle exit. Depending on the wavenumber of the interacting vortices, the final stage of pairing near the potential core would be different, leading to different observed passage frequencies.

3.2. SOUND GENERATION

The maximum sound pressures on the major and minor lobes at $m = 6$ are shown in Figures 9(a) and 9(b) respectively. As expected, the sound pressure fluctuations during the first slip through are the same as those of the unperturbed vortex interaction of $+0{\cdot}03$ and $-0{\cdot}02$ [1]. However, the sound pressures during the second slip through are significantly higher than those of the first slip through. At $t' \approx 11$, the sound pressures increase to $+0{\cdot}27$ and $-0{\cdot}24$, an order of magnitude higher than those of the first slip through and of the unperturbed case (Table 1). The isocontours of the instantaneous sound pressure p' at $t' = 13{\cdot}575$ are shown in Figure 10(a), indicating a quadrupole sound radiation. However, it does not indicate any rotation of the principal axes of the quadrupole throughout the computation, in contrast with those for $m = 1$ and 2 [1].

The maximum sound pressures on the major and minor lobes at $m = 7$ are also shown in Figures 9(a) and 9(b). After the third slip through, at $t' \approx 19$, the sound pressures increase to a magnitude as high as $+0{\cdot}11$ and $-0{\cdot}08$ (Table 1). Although they are higher than those of the unperturbed ($m = 0$) of $+0{\cdot}03$ and $-0{\cdot}02$, they are slightly lower than those of $m = 6$. The isocontours of the sound pressure of this wavenumber during the third slip through at $t' = 18{\cdot}575$ are shown in Figure 10(b), indicating also quadrupole in nature. No rotation of the principal axes of the quadrupole is observed.

Figures 11(a) and 11(b) show the maximum sound pressures on the major and minor lobes for $m = 8$. At $t' \approx 11$, the pressures can be as high as $+0{\cdot}08$ and $-0{\cdot}07$, lower than those of $m = 6$ (Table 1). The isocontours of the sound pressure

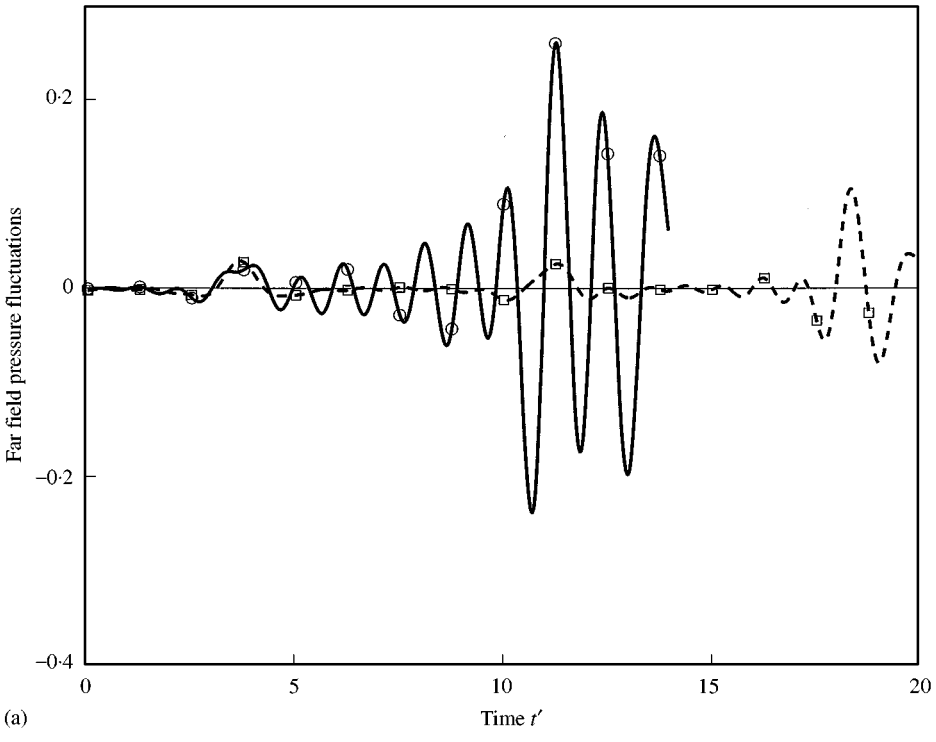

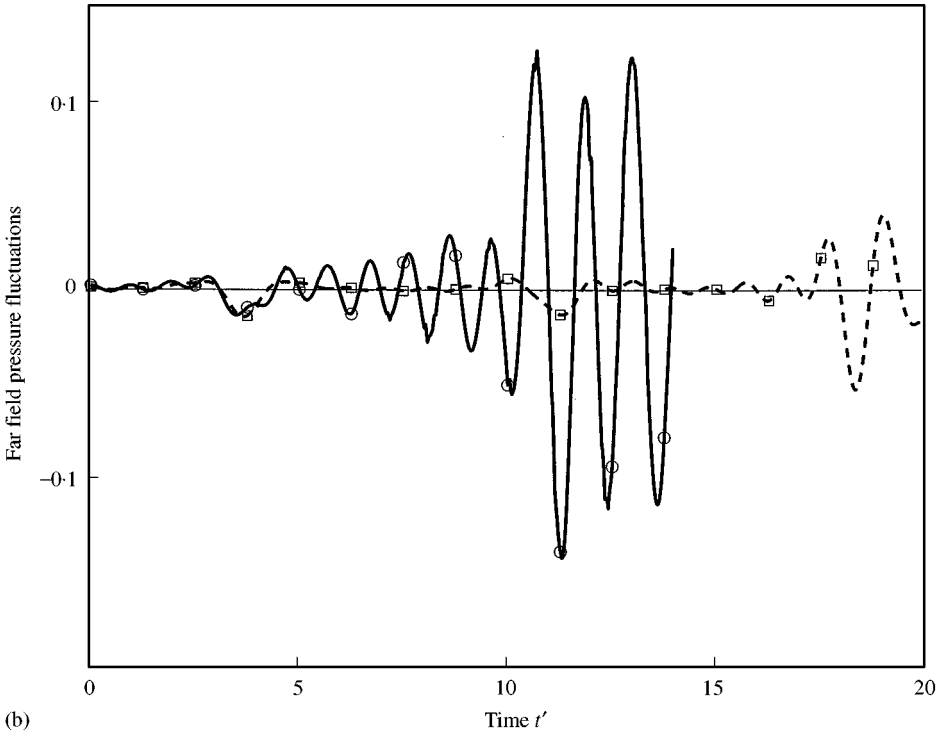

Figure 9. Maximum far field sound pressure radiated by the two interacting vortex rings. (a) Major lobe; (b) minor lobe. ○, $m = 6$; □, $m = 7$.

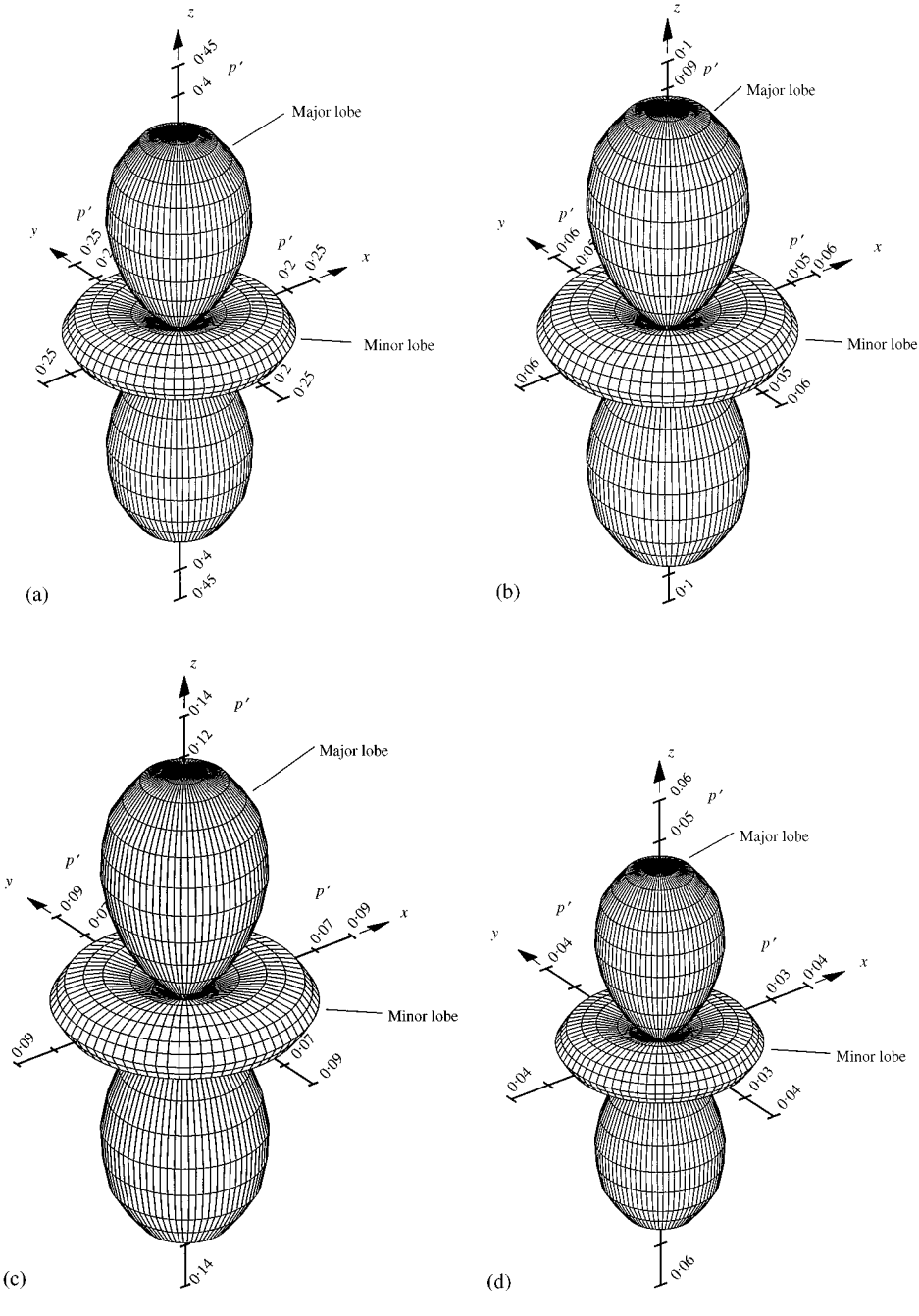

Figure 10. Isocontours of far field sound pressure. (a) $m = 6$, $t' = 13{\cdot}575$; (b) $m = 7$, $t' = 18{\cdot}575$; (c) $m = 8$, $t' = 13{\cdot}5$; (d) $m = 9$, $t' = 18{\cdot}275$; (e) $m = 10$, $t' = 15{\cdot}4$; (f) $m = 11$, $t' = 18{\cdot}575$.

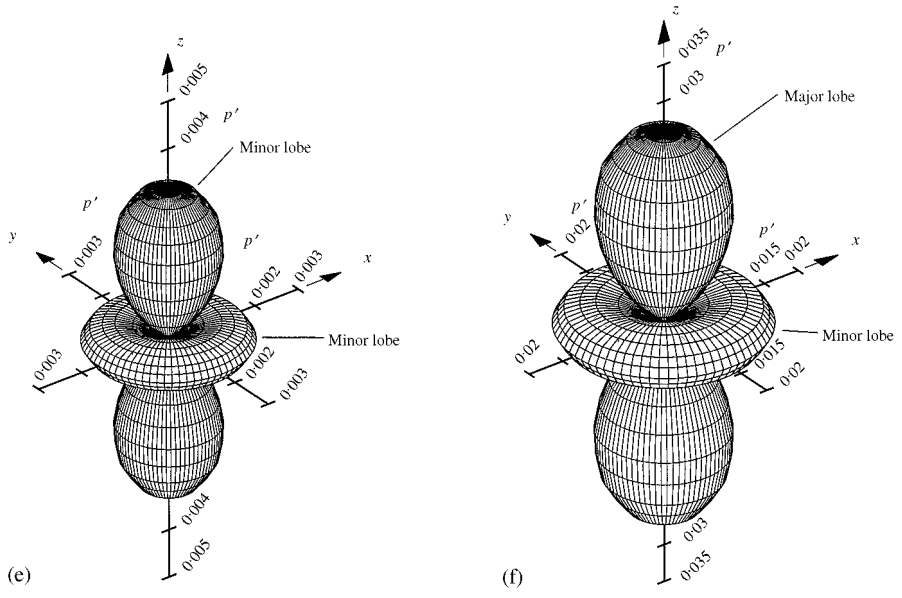

Figure 10. Continued.

of this wavenumber at $t' = 13{\cdot}5$ are shown in Figure 10(c), quadrupole in nature and without any rotation of the principal axes.

The maximum sound pressures on the major and minor lobes at $m = 9$ are also shown in Figures 11(a) and 11(b) respectively. The peak pressures are $+0{\cdot}27$ and $-0{\cdot}4$ at $t' \approx 17$ (Table 1). These pressures are slightly higher than those of $m = 5$ and 7 of the other star-like structure with tail sheaths. The isocontours of the sound pressure of this wavenumber at the third slip through instant $t' = 18{\cdot}275$ are shown in Figure 10(d), indicating quadrupole in nature. There is also no rotation of the principal axes of the quadrupole.

The maximum sound pressures on the major and minor lobes at $m = 10$ are also shown in Figures 12(a) and 12(b) respectively. The peak pressures are $+0{\cdot}18$ and $-0{\cdot}16$ at $t' \approx 14$ (Table 1). These pressures are nearly the same as those of $m = 6$ and 8 of similar roll-shape structure. The isocontours of the sound pressure of this wavenumber at $t' = 15{\cdot}4$ are shown in Figure 10(e), also indicating quadrupole with no rotation of the principal axes.

The maximum sound pressures on the major and minor lobes at $m = 11$ have the low values of $+0{\cdot}03$ and $-0{\cdot}03$ at $t' \approx 19$ (Figures 12(a) and 12(b)). They are the same as those of $m = 0$ (Table 1). However, the sound pressure fluctuations are dominated by high-frequency components, especially after the second slip through. The fluctuations of these high-frequency components are as high as the value at the slip through instant. Contrary to the unstable wavenumbers, there is no rapid increase near and after the second or third slip through at

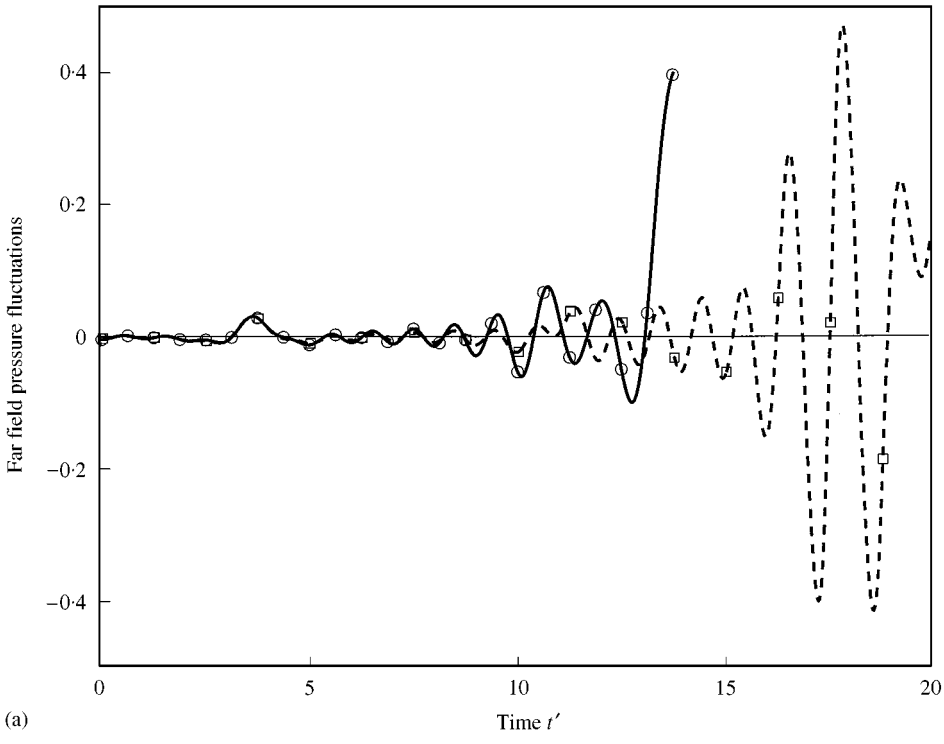

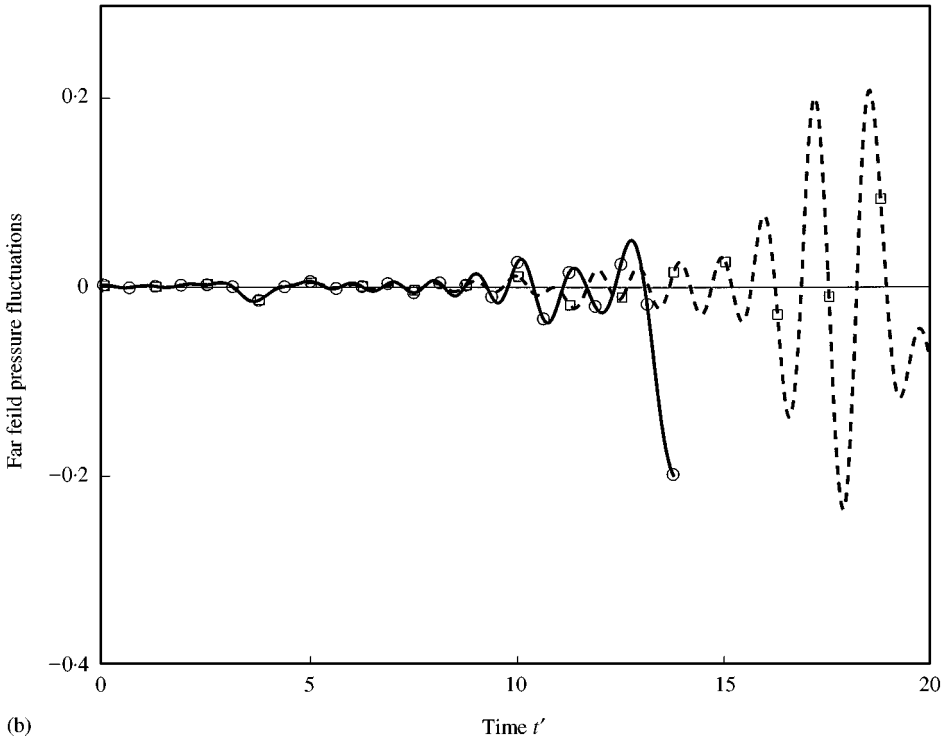

Figure 11. Maximum far field sound pressure radiated by the two interacting vortex rings. (a) Major lobe; (b) minor lobe. ○, $m = 8$; □, $m = 9$.

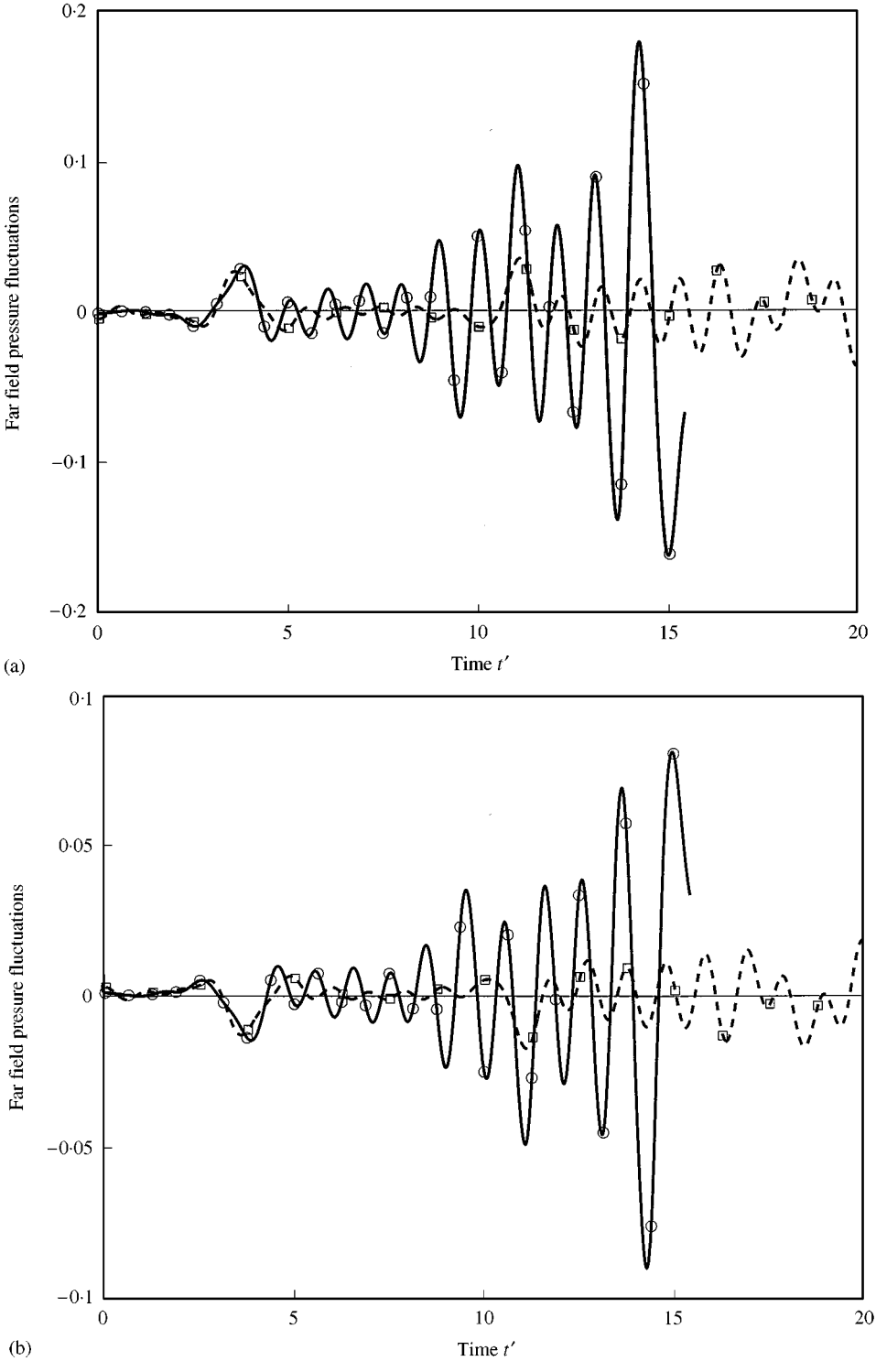

Figure 12. Maximum far field sound pressure radiated by the two interacting vortex rings. (a) Major lobe; (b) minor lobe. ○, $m = 10$; □, $m = 11$.

this wavenumber. The isocontours at the third slip through instant $t' = 18{\cdot}575$ are also of quadrupole in nature, even though the sound pressures are low (Figure 10(f)).

For the interaction of vortex rings perturbed at stable mode, the maximum sound pressures in the far field at the third slip through are $+0{\cdot}03$ and about $-0{\cdot}02$ for $m = 3$, 4 and 11 (Table 1). They are essentially the same as those of the unperturbed vortex ring interaction ($m = 0$) of $+0{\cdot}03$ and $-0{\cdot}02$. However, for $m = 11$, high-frequency sound pressure fluctuations emerge after the first slip through at $t' > 5$ (Figures 12(a) and 12(b)). This observation reveals that although the interactions of vortices perturbed at the stable mode are similar, the effect of the

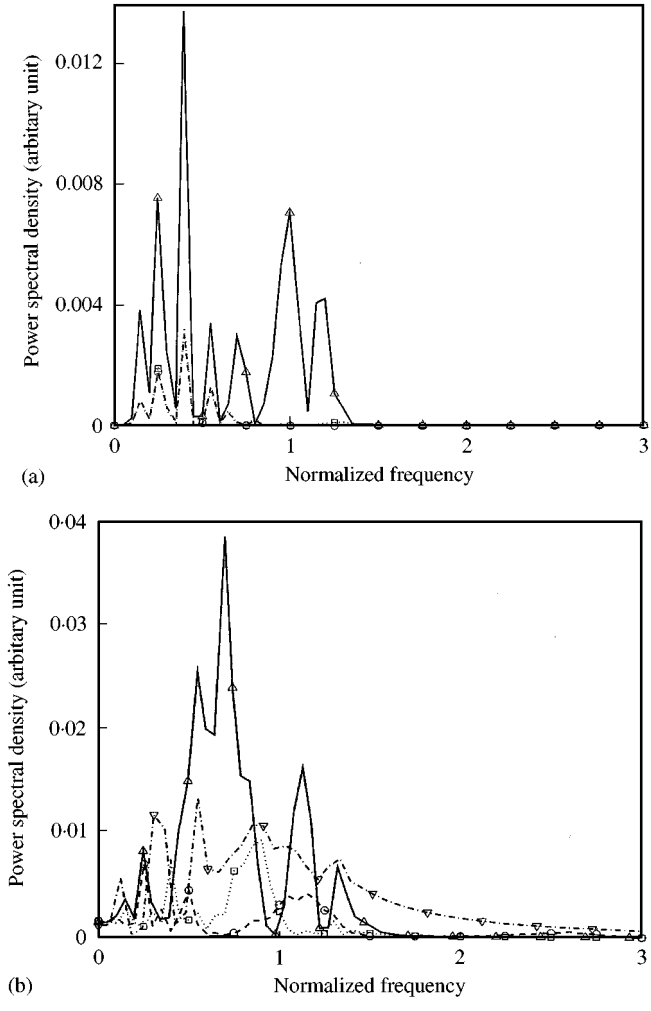

Figure 13. Spectra of far field sound pressure of major lobe at various wavenumbers. (a) Stable mode; ○, $m = 3$; □, $m = 4$; △, $m = 11$. (b) Odd-m unstable mode; ○, $m = 1$; □, $m = 5$; △, $m = 7$; ▽, $m = 9$. (c) Even-m unstable mode; ○, $m = 2$; □, $m = 6$; △, $m = 8$; ▽, $m = 10$.

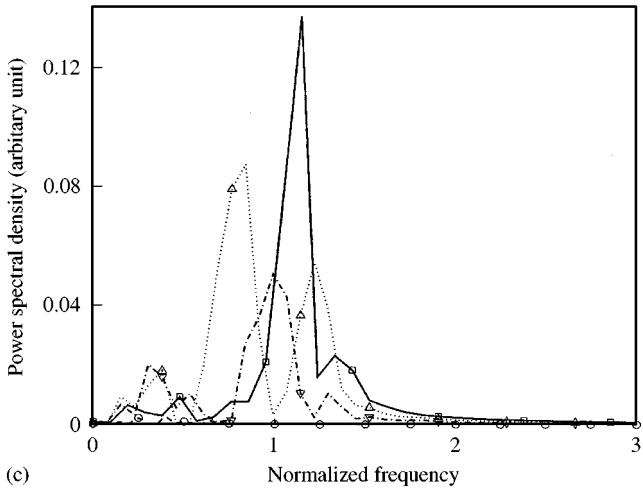

Figure 13. Continued.

wavenumber on the sound generation becomes critical at the later stage of interaction.

For the odd-m unstable mode, the maximum sound pressures at and near the third slip through are $+0{\cdot}07$ and $-0{\cdot}06$ for $m = 5$, $\pm 0{\cdot}11$ and $-0{\cdot}08$ for $m = 7$, and $+0{\cdot}27$ and $-0{\cdot}4$ for $m = 9$. They are higher than those of $+0{\cdot}03$ and $-0{\cdot}02$ of the stable mode. The sound pressure increases significantly just before the third slip through and consists also of high-frequency components. This means that for this unstable mode the high-frequency sound pressures are mainly generated around the third slip through instant at which the long tails of hairpin vortical structures begin to elongate tremendously.

For the even-m unstable mode, the maximum sound pressures are nearly the same with $+0{\cdot}27$ and $-0{\cdot}24$ for $m = 6$, and $+0{\cdot}18$ and $-0{\cdot}16$ for $m = 10$. These sound pressures are slightly lower than those of $m = 9$ but slightly higher than those of $m = 5$ and 7 of the odd-m unstable mode. For this unstable mode, high-frequency components of the sound pressure emerge after the first slip through. The high sound pressure occurs near the second slip through instant at $t' \approx 11$. This implies that the early appearance of the peak sound pressure is associated with the development of the roll-shape structure during the second slip through. For $m = 8$, the maximum sound pressure of $+0{\cdot}08$ and $-0{\cdot}07$ at $t' \approx 11$ during the second slip through are slightly lower than those of $m = 6$ and 10 (Table 1). It may be due to the lower evolution of the thin sheaths.

The sound power spectra of the three stable and unstable modes show that the peak sound power is of low level for the stable wavenumbers $m = 3$, 4 and 11 (Figure 13(a)). For the odd-m unstable mode, the spectra of $m = 1$, 5, 7 and 9 show the more intense dominant peak and the high-frequency components ($m = 1$ is included for comparison) (Figure 13(b)). The highest power occurs at $m = 9$. For the even-m unstable mode, the spectra of $m = 2$, 6, 8 and 10 are generally higher,

also of the dominant peak and the high-frequency components ($m = 2$ is included for comparison) (Figure 13(c)). Among all the wavenumbers studied, the highest power occurs at $m = 6$, at which both the leading and trailing vortices form the roll-shape structures (Figures 2(a)). Thus, it indicates that the even-m mode, in which the vortices form the roll-shape structures, is the most unstable together with its more efficient far field sound generation. However, there does not seem to be a significant difference in the frequency characteristics, except the difference in the dominant peak frequency with wavenumber, between those of the second and the third categories. This implies the difficulty in distinguishing the far field contributions by these two unstable modes of interaction of the two perturbed vortices.

The spectra in Figure 13 also demonstrate a shift of the dominant frequency of the far field vortex pairing sound to high-frequency regime. This feature explains the effective use of the corrugated nozzle as noise suppressor for the jet exhaust of pure jet and low by-pass engines [25, 26] for which the major frequency contribution to jet noise is shifted from the low to high frequencies.

4. CONCLUSIONS

The study of the interaction and sound generation of two coaxial thin vortex rings with weak azimuthal instability has been extended. The range of wavenumbers studied covers $6 \leqslant m \leqslant 11$ and the non-linear evolutions of the perturbed interacting vortices have been investigated. With the findings of a previous study [1], three perturbed vortex ring interaction modes, namely the stable mode, odd-m and even-m unstable modes, have been identified. The stable mode interaction closely resembles the unperturbed vortex ring interaction. The odd-m mode interaction ends up with the formation of a severely stretched vortex ring with vortical tails extending downstream. The even-m mode results in the roll-shape vortical structures. The occurrence of the interaction modes depends critically on the value of m and this dependence can explain the diversity of the three-dimensional development of the vortex rings as observed in the experiments.

The sound generation in the far field by the perturbed vortex interaction has been computed. Besides the sound pulses due to the slip through motion, the sound pressure fluctuations are dominated by high-frequency components. These high-frequency components become dominant at the later stages of interaction at which the non-linear evolutions of the vortices are found.

ACKNOWLEDGMENTS

This study is partly supported by a grant from the Research Grants Council, Hong Kong. The second author was awarded a Croucher Fellowship by the Croucher Foundations.

REFERENCES

1. R. C. K. Leung and N. W. M. Ko 1997 *Journal of Sound and Vibration* **202**, 1–27. The interaction of perturbed vortex rings and its sound generation.
2. O. M. Knio and A. F. Ghoniem 1990 *Journal of Computational Physics* **86**, 75–106. Numerical study of a three-dimensional vortex method.
3. W. Möhring 1978 *Jounral of Fluid Mechanics* **85**, 685–691. On vortex sound at low mach number.
4. S. E. Widnall and J. P. Sullivan 1973 *Proceedings of the Royal Society of London* **A332**, 335–353. On the stability of vortex rings.
5. P. G. Saffman 1982 *Vortex Dynamics*. Cambridge: Cambridge University Press.
6. G. K. Batchelor 1967 *An Introduction to Fluid Dynamics*. Cambridge: Cambridge University Press.
7. G. Winckelmans and A. Leonard 1993 *Journal of computation Physics* **109**, 247–273. Contributions to vortex particle methods for the computation of three-dimensional incompressible unsteady flows.
8. S. E. Widnall, D. B. Bliss and C. Y. Tsai 1974 *Journal of Fluid Mechanics* **66**, 35–47. The instability of short waves on a vortex ring.
9. P. G. Saffman 1978 *Journal of Fluid Mechanical* **84**, 625–639. The number of waves on unstable vortex rings.
10. M. Dziedzic and H. J. Leutheusser 1996 *Experiments in Fluids* **21**, 315–324. An experimental study of viscous vortex rings.
11. A. Weigand and M. Gharib 1997 *Experiments in Fluids* **22**, 447–457. On the evolution of laminar vortex rings.
12. A. Weigand 1996 *Experiments in Fluids* **20**, 358–364. Simultaneous mapping of the velocity and deformation field at a free surface.
13. J. E. Martin and E. Meiburg 1991 *Journal of Fluid Mechanics* **230**, 271–318. Numerical investigation of three-dimensionally evolving jets subject to axisymmetric and azimuthal perturbations.
14. T. T. Lim 1997 *Physics of Fluids* **9**, 239–241. A note on the leapfrogging between two coaxial vortex rings at low Reynolds numbers.
15. J. D. Swearingen, J. D. Crouch and R. A. Handler 1995 *Journal of Fluid Mechanics* **291**, 1–28. Dynamics and stability of a vortex ring impacting a solid boundary.
16. A. J. Yule 1978 *Journal of Fluid Mechanics* **89**, 231–269. Large-scale structure in the mixing layer of a round jet.
17. H. E. Fiedler 1988 *Progress in Aerospace Sciences* **25**, 231–269. Coherent structures in turbulent flows.
18. E. Meiburg, J. C. Lasheras and J. E. Martin 1991 *Turbulent Shear Flows* **7**, 195–208. Berlin: Springer. Experimental and numerical analysis of the three-dimensional evolution of an axisymmetric jet.
19. P. A. Monkewitz, D. W. Bechert, B. Barsikow and B. Lehmann 1990 *Journal of Fluid Mechanics* **213**, 611–639. Self-excited oscillations and mixing in a heated round jet.
20. C. O. Paschereit, D. Oster, T. A. Long, H. E. Fiedler and I. Wygnanski 1992 *Experiments in Fluids* **12**, 189–199. Flow visualization of interactions among large coherent structures in an axisymmetric jet.
21. D. Liepmann and M. Gharib 1992 *Journal of Fluid Mechanics* **245**, 643–668. The role of streamwise vorticity in the near-field entrainment of round jets.
22. G. Broze and F. Hussain 1996 *Journal of Fluid Mechanics* **311**, 37–71. Transitions to chaos in a forced jet: intermittency, tangent bifurcations and hysteresis.
23. F. O. Thomas 1991 *Applied Mechanics Reviews* **44**, 119–153. Structure of mixing layers and jets.
24. E. Gutmark and C. M. Ho 1983 *Physics of Fluids* **26**, 2932–2938. Preferred modes and the spreading rates of jets.

25. M. J. T. Smith 1989 *Aircraft noise*. Cambridge: Cambridge University Press.
26. P. R. Gliebe, J. F. Brausch, R. K. Majjigi and R. Lee 1995 *Aeroacoustics of Flight Vehicles*: *Theory and Practice*, *Vol.* 2: *Noise Control*. (H. H. Hubbard, editor) (207–270). New York: Acoustical Society of America. Jet noise suppression.